Zebrafish *bmp10* Mutants as a Model for Hereditary Hemorrhagic Telangiectasia - Associated High Output Heart Failure

by

Bijun Li

BS, Jinan University, China, 2007

MS, Jinan University, China, 2010

Submitted to the Graduate Faculty of

Human Genetics

Graduate School of Public Health in partial fulfillment

of the requirements for the degree of

Master of Science

University of Pittsburgh

2019

UNIVERSITY OF PITTSBURGH

GRADUATE SCHOOL OF PUBLIC HEALTH

This thesis was presented

by

Bijun Li

It was defended on

March 28, 2019

and approved by

Zsolt Urban, PhD, Associate Professor, Department of Human Genetics, Graduate School of Public Health, University of Pittsburgh

Bernhard Kuhn, MD, Associate Professor and Director of Research in Cardiology, Department of Pediatrics, School of Medicine, University of Pittsburgh

Cynthia St Hilaire, PhD, Assistant Professor of Medicine, Division of Cardiology, Vascular Medicine Institute, School of Medicine, University of Pittsburgh

Thesis Advisor: Beth L. Roman, PhD, Associate Professor, Department of Human Genetics, Graduate School of Public Health, University of Pittsburgh

Zebrafish *bmp10* Mutants as a Model for Hereditary Hemorrhagic Telangiectasia - Associated High Output Heart Failure

Bijun Li, MS

University of Pittsburgh, 2019

Abstract

Hereditary hemorrhagic telangiectasia (HHT) is an inherited disease caused by impaired signaling through the bone morphogenetic protein (BMP) receptor, ALK1, and is characterized by fragile, direct connections between arteries and veins, called arteriovenous malformation (AVMs). AVMs can form in skin, mucous membranes, brain, lung, and liver and can be life-threatening if severe shunting or rupture occurs. For example, severe liver AVMs result in low systemic vascular resistance, which can lead to a transient, compensatory high-output cardiac state followed by decompensation and heart failure. The only treatment for HHT-associated high-output heart failure (HOHF) is liver transplant. As such, the need for targeted therapeutics is clear, yet little is known about the pathological progression of HOHF. Here, I describe zebrafish *bmp10* mutants as a useful animal model of HHT-associated, age-dependent HOHF. *bmp10* encodes one of three Alk1 ligands in zebrafish, and homozygous *bmp10* mutants develop dilated and hemorrhagic skin vessels, edema, and enlarged hearts as early as six weeks of age. *bmp10* mutants with severe early-onset vascular phenotype exhibit high cardiac output, cardiomyocyte (CM) disorganization, and early death, whereas those with later-onset vascular lesions show milder heart phenotype. At the cellular level, *bmp10* mutant hearts may have CM hypertrophy and increased proliferating cell nuclear antigen (PNCA) signal. Our long-term goal is to use this zebrafish model to understand the mechanisms involved in cardiac compensation and in the pathological progression to heart failure, which may aid in design of medical therapies to prevent HOHF in HHT patients. Also, in addition

to HHT, HOHF is identified in some common diseases, such as morbid obesity, anemia and sepsis, and HOHF is associated with high mortality. Hence, studying this type of heart failure is of public health significance.

Table of Contents

List of Tables

List of Figures

Preface

I would like to thank Dr. Beth Roman for mentoring me. I have learnt not only the science concepts and techniques in her lab, but also from her meticulousness and integrity in her work. I would also like to thank the Roman lab members for their helps and encouragement. I always remember the joy we share together.

I would like to thank our collaborators Dr. Kang Kim and Dr. Villanueva Flordeliza for their excellent echocardiography skills. I give tremendous thanks to the Kim lab members Xiaozhou Fan, Harry Volek and Waqas Bin Khalid for all the efforts they put into the zebrafish ultrasound project.

I am grateful that Dr. Simon Watkins and the specialists from Center for Biologic Imaging teach me in confocal imaging, TEM and various other techniques that I was totally new to.

Thanks to my committee members Dr. Bernhard Kuhn, Dr. Cynthia St Hilaire and Dr. Zsolt Urban for providing their expertise and insights into my projects. Thanks to Dr. Candace Kammerer for her academic advice and mentoring throughout my graduate school journey.

Last but not least, I thank my friends and family for their supports, encouragement, and prayers. I am blessed to have had many mentors in my church to keep me positive and to see the great meaning of my work, so I give many thanks to all of them.

1.0 Background and Significance

1.1 Introduction to Heart Failure

Heart failure is a global public health problem, laying a substantial burden on society, family and the individual. Heart failure affects at least 26 million people worldwide, and its prevalence keeps increasing as the population ages. Mortality and morbidity are high, and expenditure is vast due to the high hospitalization rate and related health care cost (Savarese & Lund, 2017). Clinical and basic research in cardiology have been growing vigorously in attempt to develop therapeutics that can prevent or slow down the heart failure process. This goal drives us to better classify the types of heart failure, study their etiology, and conduct mechanistic analysis of disease progression. Based on the clinical descriptions of cardiac output, heart failure can be classified as low output heart failure (LOHF) or high output heart failure (HOHF).

LOHF is common and is further subtyped as systolic heart failure and diastolic heart failure. The underlying mechanism in systolic heart failure is the heart not being able to pump adequately. The left ventricular muscle weakens, and the left ventricle is not pumping with enough force to allow normal circulation. Systolic heart failure may be caused by high blood pressure, coronary artery disease, or myocardial infarction. Systolic heart failure is also clinically called heart failure with reduced ejection fraction, in which there is an increase in end systolic volume while also a greater increase in end diastolic volume. The left ventricle shape changes from ellipsoidal to globular (Chatterjee, 2012). Also, the left ventricle cavity increases while its wall thickness may be unchanged or decreased. These two findings are associated with an increase in wall stress (Chatterjee, 2012). The increased wall stress together with the impaired contractility

causes the reduced ejection fraction. Left ventricular dilation may progressively worsen in patients without adequate pharmacotherapy treatment and may lead to more severe heart failure. In systolic heart failure, abnormal collagen deposition is also observed in the left ventricle tissue (Rossi et al., 2004).

In diastolic heart failure, left ventricular muscle stiffens and increases resistance against filling. Diastolic heart failure is caused by high blood pressure, aging, diabetes, and other causes. In clinic, a normal ejection fraction is observed in diastolic heart failure, thus it is also called heart failure with preserved ejection fraction. The preserved ejection fraction is attributed to decreased end-systolic and end-diastolic volumes. Diastolic heart failure is characterized by increased left ventricular wall stiffness and/or thickness, and increased cardiomyocyte (CM) size (Aurigemma, Zile, & Gaasch, 2006). There is also an increase in collagen bundle thickness, but the collagen volume remains normal (Aurigemma, Zile, & Gaasch, 2006).

HOHF is rare. It is a condition in which the heart, in an effort to generate high cardiac output to maintain blood pressure, exceeds its pumping capacity and progresses to heart failure. In healthy people, high cardiac output temporarily occurs during exercise, in order to meet the increased demand for oxygen and energy. In some disease conditions, high cardiac output persists and eventually leads to heart failure. The underlying disease states include chronic anemia, chronic hypercapnia, sepsis, and systemic arterio-venous fistula. Except for cardiomegaly, there is little known about the structural change in HOHF. However, the underlying pathophysiology is clear. Vasodilation or arteriovenous shunts lead to reduced systemic vascular resistance and thus a fall in arterial blood pressure (Mehta & Dubrey, 2009). Low arterial blood pressure results in neural hormonal activation, which includes activation of the sympathetic nervous system and the renin-angiotensin-aldosterone system (RAAS). In this response, sympathetic activation leads to

increased heart rate and increased vasoconstriction, and over time, ventricular remodeling, which increases stroke volume which in turn increases arterial blood pressure. RAAS activation results in water and salt retention, and thus the expansion of the blood volume, another strategy to increase arterial blood pressure. Despite the increased heart rate and increased stroke volume, the ejection fraction may be unchanged because of the proportional increases in end-systolic volume and end-diastolic volume. Compensatory left ventricular dilation and/or hypertrophy may progress to heart failure.

1.2 HOHF Pathogenesis: HHT and AVMs

HHT has a broad spectrum of manifestations and highly variable expressivity. Although the primary defect is the presence of AVMs, they can form at multiple sites affecting different organs, and the dilation or rupture of the vessels can lead to secondary and tertiary consequences (Shovlin, 2015). Liver AVMs are associated with one of the most severe secondary consequences, HOHF. Patients with liver involvement can have a cardiac index (CI, cardiac output/body surface area,) > 3.9 L/min/m^2 (Anand & Florea, 2001), while the normal range for CI is 2.5-4 L/min/m^2 .

In HHT, liver involvement manifests as disseminated intrahepatic telangiectasias and shunting from the hepatic artery to the hepatic veins (Garcia-Tsao, 2007). The reduced systemic vascular resistance causes a fall in arterial blood pressure, which leads to the activation of the neural hormonal system. Moreover, the organs in which AVMs form suffer tissue hypoxia and insufficient metabolism due to lack of oxygen and nutrition exchange through capillary bed, another factor that stimulates neural hormonal changes. Also, AVMs at other sites, such as the nose and GI tract, are easily ruptured by the high blood flow, resulting in hemorrhages, anemia,

and a further reduced arterial oxygen content. All these physiological factors contribute to increased stroke volume (Shovlin, 2015). To date, the only proven therapy for HOHF is liver transplantation. Conventional therapies for low-output heart failure are ineffective because they have vasodilatory properties, which will further decrease the vascular resistance (Mehta & Dubrey, 2009). Therapeutic strategies for treating HOHF include preventing formation of AVMs or preventing heart failure progression. This calls for a deeper mechanistic understanding of HHT and HOHF.

1.3 HHT Genetics

Mutations in *ENG, ACVRL1,* and *SMAD4* are responsible for HHT (McAllister et al., 1994; Johnson, et al., 1996; Gallione, et al., 2004). They encode BMP signaling pathway components that act in endothelial cells (ECs) lining blood vessel. In normal signal transduction (Roman & Hinck, 2017), circulating BMP ligands bind to the type I receptor serine/threonine kinase, ACVRL1 (also called ALK1), in concert with type Ⅱ receptor serine/threonine kinases, BMPRII, activin receptor A or activin receptor B. Ligand binding is aided by the non-signaling type Ⅲ receptor, endoglin (ENG). The type Ⅱ receptors phosphorylate the type Ⅰ receptor, ALK1, which then phosphorylates SMAD1, SMAD5, or SMAD8 in the cytoplasm. Phosphorylated SMAD1/5/8 proteins recruit the common partner SMAD4 and enter the nucleus and regulate gene expression. In HHT, patients are heterozygous for one of the three genes, indicative of haploinsufficiency. Therefore, one therapeutic strategy for HHT is to enhance BMP signaling in endothelial cells via increasing circulating BMP ligand to activate the remaining functioning receptor. BMP9 and

BMP10 are two known ligands with high affinity to ALK1 receptor (Brown et al., 2005; David et at., 2007), but evidence suggests they might have functional redundancy (Chen et al., 2013). To identify the physiological ligand(s), our lab generated zebrafish mutant lines *bmp9*, *bmp10*, and *bmp10*-like (a paralog to *bmp10* in zebrafish). In our ligand requirement study, we found a unique and surprising requirement for zebrafish *bmp10*: *bmp10* mutants develop an adult phenotype highly similar to HHT patients, including skin, liver and heart involvement.

1.4 Zebrafish Model for HHT: *alk1* and *bmp10* mutants

1.4.1 *alk1* mutants as an HHT model

Using zebrafish *alk1* mutants as an HHT model, we have gained insight into how disruption of *alk1* leads to AVMs. Our *alk1* mutant line was isolated in a forward genetic screen (Driever et al., 1996). *alk1* mutants nicely phenocopy HHT vasculature, exhibiting AVMs in cranial vessels at 2 days post-fertilization with complete penetrance (Roman et al., 2002). In a previous study (Rochon, Menon, & Roman, 2016), we showed that loss of *alk1* alters EC migration in the arteries proximal to heart. In wild type embryos, ECs in cranial arteries migrate against blood flow, while in *alk1* mutants, the EC migration against flow is weakened and EC migration in the direction of blood flow is enhanced. This phenomenon results in increased EC number in and caliber of distal arterial segments. AVMs then form downstream of enlarged, Alk1-positive vessels in the presence of blood flow: at least one normally transient arterial-venous blood vessel segment is aberrantly retained (Corti et al., 2011), likely in response to increased shear stress.

Alk1 ligands in zebrafish

As introduced above, zebrafish have three Alk1 ligands: Bmp9, Bmp10 and Bmp10-like. Bmp10 and Bmp10-like are likely duplicates that arose as a result of a whole-genome duplication event in teleost (Woods et al., 2005). At the protein level, the growth factor domain of Bmp10-like is 63.3% identical to Bmp10. To investigate Alk1 ligand requirements, our lab generated *bmp9, bmp10*, and *bmp10-like* mutants: no single mutant shows abnormal vessel formation, confirming our previously published knockdown results (Laux et al., 2013). However, combined loss of *bmp10* and *bmp10-like* phenocopies *alk1* mutants, suggesting that both genes encode Alk1 ligands with functional redundancy (T. Capasso and B. Roman, unpublished).

Despite the fact that *bmp10* and *bmp10-like* paralogs are redundant with respect to embryonic vascular development, expression patterns suggest the possibility of subfunctionalization: *bmp10* is expressed in endocardium and *bmp10-like* in myocardium at 36 hours post-fertilization (Laux et al., 2013). Observation of these mutants throughout life bears out this prediction: *bmp10* mutants develop a distinct cardiovascular phenotype during the juvenile to adult period.

1.4.2 Identification of adult phenotype in *bmp10* mutants

1.4.2.1 *bmp10* mutant phenotype

Zebrafish *bmp10* mutants show dilated skin vessels and/or abdominal edema as early as 6 weeks. Phenotype onset spans a wide range of age and presents with variable expressivity. Before 3 months, the most frequently seen external phenotype is abdominal edema with sparse skin hemorrhages; internally, these fish have ascites and pale liver and other organs. In a minority of phenotypic *bmp10* mutants, edema resolved to some extent, while most of those with edema

became progressively worse and died before 3 months (B. Li, data not shown). At 5 months, some *bmp10* mutants grew to a similar size as their wild type (WT) siblings, exhibiting dilated anterior vessels and hemorrhages (Fig. 1A). Other mutant fish were short and thin, while some appeared larger with edema, and others were indistinguishable from wild type siblings. In addition to eternal vascular lesions, at 5 months, some *bmp10* mutants had a plexus-like vessel network and dilated arteries in the liver (Fig. 1B). At 12 months, most mutants only had slightly dilated vasculature in the head, while those with severe hemorrhages were rare.

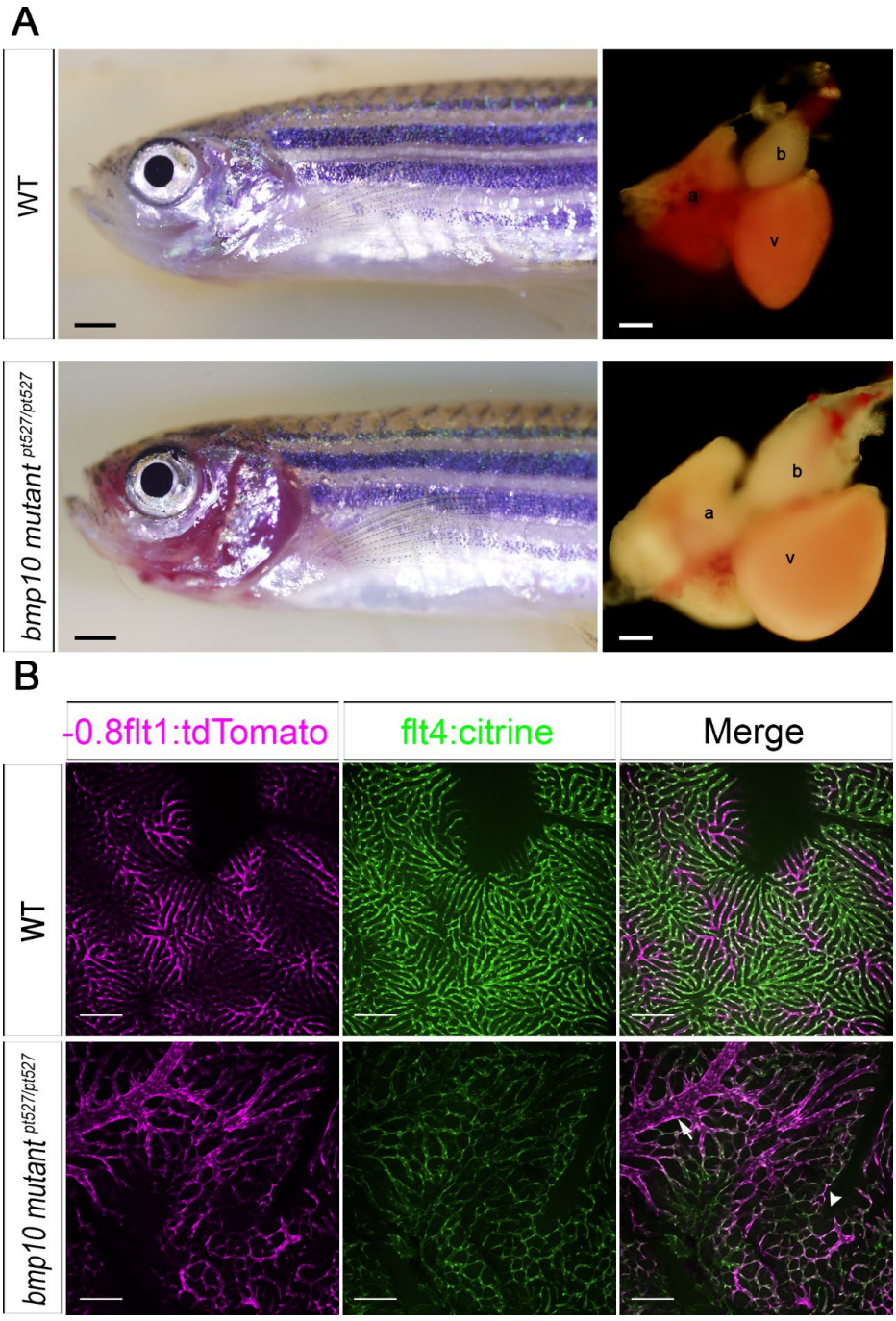

Figure 1. *bmp10* mutant vessel and heart phenotype at 5 months.

(A) In comparison with the normal appearance of the WT sibling, *bmp10* mutant shows dilated vessels and hemorrhages in the anterior. Scale bars: 1 mm. Normal heart and enlarged and abnormally shaped heart from the fish in the left. Scale bars: 200 μm. a, atrium; v, ventricle; b, bulbus arteriosus.
(B) Liver vessel images show *bmp10* mutant has dilated arteries (arrow) and plexus-like network (arrowhead). Arteries are in magenta and veins in green. Scale bars: 100 μm. N = 3 (WT) and 6 (*bmp10* mutant); 1 experiment.

1.4.2.2 Correlation of vessel and heart phenotypes in *bmp10* mutant

At all time points, when the heart is dissected from externally phenotypic *bmp10* mutants, an irregular ventricular shape with or without enlargement is consistently seen, while non-phenotypic *bmp10* mutant hearts seem normal. A close correlation between the severity of vessel defects and heart abnormality is observed. This leads us to hypothesize that the *bmp10* mutant heart is adapting to the altered volume and pressure of blood flowing through the abnormal vascular structure, mimicking the HOHF phenotype in human patients.

1.4.3 Zebrafish as a model for cardiac disorders

Zebrafish can serve as a valuable in vivo model for investigating acquired or heritable cardiac disorders. Cardiac remodeling in response to hemodynamic changes has been demonstrated in an anemia-induced HOHF model (Sun et al., 2009). Also, adult fish have been used to study the progression of cardiac disease caused by environmental assault. For example, adult zebrafish show consistent heart failure by chronic isoproterenol activation on β-adrenergic receptor (β-AR), displaying similar changes on functional and molecular levels to mammals (Kossack et al., 2017). What is more, based on embryonic studies, zebrafish mutants show heart phenotypes involving the contractile machinery and rhythmicity, which resemble the characteristics of human cardiac disease (Nguyen, Lu, Wang, & Chen, 2008). These observations support the notion that the mechanisms regulating these processes are conserved from fish to mammal. Developmentally, the zebrafish heart and the mammalian heart undergo similar morphogenetic processes (Nguyen, Lu, Wang, & Chen, 2008). After heart tube formation and looping, both fish and mammals develop cardiac ridges protruding from the ventricle wall, a process called trabeculation (Sedmera & Thomas, 1996). Fish hearts remain trabeculated

throughout life while mammalian hearts get compacted at a later stage of development (Burggren et al., 1991). Another difference between fish and mammalian hearts is that the fish heart only has two chambers, atrium and ventricle, with no septum dividing the chambers (Burggren et al., 1991). One other unique characteristic of the zebrafish heart is its ability to regenerate throughout life. Zebrafish CMs are capable of proliferating and repairing cardiac injury without leaving a scar (review by González-Rosa et al., 2017). Despite these differences, the zebrafish heart is a valuable model of human heart disease.

1.5 BMP10's Documented Role in Cardiovascular System

BMP10 has dual roles in vessel and heart development in mouse (Chen et al., 2004; Chen et al., 2013). *Bmp10* knockout mice show embryonic fusion of artery and vein, and abnormal vasculature in yolk sac, suggesting its crucial role in embryonic vascular development (Chen et al., 2013). BMP10 also regulates the outgrowth of myocardium in both embryonic and postnatal heart in mouse (Chen et al., 2004; Chen et al., 2006). Whole-mount in situ hybridization on mouse embryos shows *Bmp10* is exclusively expressed in embryonic heart. Its expression is first confined to developing ventricular trabeculae at E9.0 and then shifts to the atrial wall at E13.5 (Neuhaus, Rosen, & Thies, 1999). Knockout experiment provides further evidence to support BMP10's role in trabeculae outgrowth (Chen et al., 2004). *Bmp10*-deficient hearts fail to develop ventricular trabeculae at E9.5 and show acellular endocardial cushions. Overexpression provides another approach to assess BMP10's role in postnatal myocardium (Chen et al., 2006). *Bmp10* expression, driven by an α-myosin heavy chain (α-MHC) promoter that is activated specifically in postnatal myocardium, results in a significantly smaller heart, and this defect is solely due to inhibited

normal cardiomyocyte hypertrophy, while the cardiomyocyte number is not different compared to WT siblings.

It is known that BMP10 can bind to ALK1, but the BMP10 receptors in the heart remain unclear. BMP10 has a high affinity for ALK1, and it has been shown that ALK1 can transduce BMP10 signaling in the endothelial cells (Castonguay et al., 2011). As for the heart, *Alk3* and *Alk6* are both expressed in the murine postnatal heart, but *Alk1* is not. Both ALK3 and ALK6 can transduce BMP10 signaling in MC3T3 cells (Mazerbourg et al., 2005). It is believed that ALK3 is a stronger candidate for BMP10 cardiac receptor than ALK6, as ALK3 expression is 1000-fold higher than ALK6 in postnatal mouse hearts (Mazerbourg et al., 2005). It has also been shown that *Alk3* is required for the normal development of trabeculated myocardium, compact myocardium, and endocardial cushions in mouse (Gaussin et al., 2002), while ALK6 is associated with a BMP2-mediated atrioventricular canal endocardium transformation in chick (Okagawa, Markwald, & Sugi, 2007).

1.6 HOHF and Public Health

The causes of HOHF are collectively common, including anemia, sepsis, obesity, liver disease, vasodilation and AVMs (Reddy et al., 2016). HOHF is secondary to these conditions, and its prevalence is highly related to them. However, HOHF may not be detected at early stages or properly diagnosed. Patients with conditions that can cause HOHF may have high cardiac output but no symptoms of clinical heart failure (Reddy et al., 2016); nevertheless, this state could progress to decompensation and become life-threatening. What is more, HOHF exhibits preserved ejection fraction, and if cardiac output is not assessed in patients, they may be misdiagnosed with

low output systolic heart failure, leading to inappropriate treatment (Reddy et al., 2016). Currently there is no proven therapy directly treating HOHF, and it can only be alleviated by correcting the underlying etiology: in the case of HHT, this means liver transplantation. Therefore, it is necessary to include the diagnostic evaluation and continued monitoring of HOHF when treating patients for conditions associated with this underrecognized disease. From the public health perspective, increasing awareness of HOHF is needed.

1.7 Significance

If we validate zebrafish *bmp10* mutants as a model for HOHF, it will enable us to gain valuable insight into the course of heart failure progression. It is unclear on the cellular and molecular level the changes that occur during the compensatory to decompensatory transition phase of HOHF. Once we understand the mechanism underlying the progression, we could target some dysregulated molecular pathway and develop therapeutics. Furthermore, if we characterize the molecular changes in HOHF with zebrafish *bmp10* mutants, we may find specific biomarkers to aid diagnosis.

1.8 Objectives

Zebrafish *bmp10* mutants provide a unique opportunity to analyze the effect of dilated vessels on the normally developed heart, thanks to the subfunctionalization of *bmp10* paralogs. In this study, my goal was to determine whether the cardiac phenotype in *bmp10* mutants represents

HOHF. This is important as we clarify the etiology of the abnormal heart. We reason that if our data show high cardiac output, it strongly suggests the heart is adapting to the dilated vasculature. To address this question, we performed echocardiography on adult zebrafish, allowing us to assess heart function and compare the zebrafish findings with those of human HOHF.

Specific Aim 1: Determine whether *bmp10* mutant hearts exhibit a high output state.

Hypothesis: To adapt to the reduced vascular resistance, the *bmp10* mutant heart generates a high cardiac output.

Method: In collaboration with Dr. Kang Kim in the Department of Medicine and Bioengineering, we used a high-resolution small animal ultrasound imaging scanner (Vevo2100, Fujifilm Visual Sonics) to measure stroke volume and cardiac output.

Specific Aim 2: Use *bmp10* mutant as a model to understand the pathophysiology of HOHF.

2a. Characterize the morphological features of the *bmp10* mutant heart.

Hypothesis: If *bmp10* mutant has high cardiac output, the heart may change its muscle layers' morphology to increase the pumping capacity.

Method: To gain a whole picture of the *bmp10* mutant heart, I used histochemistry to analyze histology and transmission electron microscopy (TEM) to assess cellular ultrastructure.

2b. Study the cellular changes in the progression of HOHF

The cardiac remodeling process in HOHF is largely unknown. Probing the cellular progression may help us understand the pathophysiology and lay a foundation for developing a specific therapy.

Method: I assessed CM proliferation, shape, size, sarcomere organization, and nucleus number in *bmp10* mutant heart.

2.0 Material and Methods

2.1 Fish Husbandry and Fish Size Standardization

Zebrafish were maintained according to standard protocol and used in experiments approved by Institutional Animal Care and Use Committee of University of Pittsburgh.

As zebrafish growth rate is largely affected by the stocking density, we maintained the tank density as larvae grew for both *bmp10* mutant and the WT siblings. After embryos were handled using standard methods, larvae from 5 days to 6 weeks post-fertilization were moved to system and grown at 40 fish/2.8 liter tank, and juveniles after 6 weeks were maintained at 20 fish/2.8 liter tank, by supplementing with age-matched Glofish.

bmp10^{pt527} allele in zebrafish was genotyped as follows. PCR primers used were Forward: CAAAGTAGCCCCATCAGCTC; Reverse: CTTCAGGGTCTCCATCAAGC.
PCR products were digested with BstNI restriction enzyme in NEB2.1 buffer (New England Biolabs) and run on 3% Metaphor gel (Lonza). *bmp10* mutants would show one band at 138 bp, while WT siblings two bands at 94 bp and 44 bp.

2.2 Zebrafish Echocardiography

Experiment setting

Zebrafish echocardiography was performed as described in a previous study (Wang et al., 2017), with minor modifications. We used a lower dose of tricaine than previously suggested to

induce and maintain anesthesia in both *bmp10* mutant and WT siblings, as *bmp10* mutants are overly sensitive to anesthesia. We induced anesthesia by putting zebrafish in 0.45 mmol/L tricaine-system water for 2 minutes, maintained the fish in 0.36 mmol/L tricaine for 2 minutes, and performed the scan in the same solution. It took 5 minutes to scan each fish. We performed echocardiography using a Vevo 2100 imaging system (FujiFilm VisualSonics, Toronto, Canada) equipped with a high frequency linear array transducer (MS 700, with bandwidth 30-70 MHz, centered operating frequency at 50 MHz).

Image analysis

We derived cardiac measurements from the ultrasound images with Vevo LAB software (FujiFilm VisualSonics) using the previously published procedure for heart rate, ventricular outflow velocity, end-systolic, and end-diastolic diameter in longitudinal view. Fractional shortening is calculated as FS = (end-diastolic diameter - end-systolic diameter)/end-diastolic diameter (Wang et al., 2017). As for stroke volume, we reasoned that as the zebrafish ventricle is highly trabeculated, it is more accurate to measure it by pulsed waveform Doppler. It is based on measurement of the ventricular outflow tract area and the range of velocities of blood flow across that area, also known as velocity time integral: stroke volume = ventricular outflow tract area × velocity time integral. To standardize stroke volume, we indexed stroke volume to the fish body weight.

2.3 Transmission Electron Microscopy

Zebrafish hearts were dissected and briefly rinsed in Ringer's solution. They were then fixed in cold 2.5% glutaraldehyde in 0.01 M PBS for at least one hour. The hearts were rinsed in

PBS, post-fixed in 1% osmium tetroxide with 1% potassium ferricyanide, rinsed in PBS, dehydrated through a graded series of ethanol and propylene oxide and embedded in Poly/Bed® 812 (Luft formulations). Semi-thin (300 nm) sections were cut on a Leica Reichart Ultracut, stained with 0.5% Toluidine Blue in 1% sodium borate and examined under the light microscope. Ultrathin sections (65 nm) were stained with uranyl acetate and Reynold's lead citrate and examined on JEOL 1011 transmission electron microscope (grant # 1S10RR019003-01 NIH for Simon Watkins) with a side mount AMT 2k digital camera (Advanced Microscopy Techniques, Danvers, MA).

2.4 Extracellular Matrix Component Staining

Zebrafish hearts were fixed in Bouin's solution at 4°C overnight and processed through standard paraffin embedding procedure. 5 μm sections were cut on a microtome and mounted on positively charged glass slides (Shandon™ ColorFrost™ Plus Slides).

Before subjected to ECM component staining, sections were deparaffinized by toluene and rehydrated through a graded series of ethanol and PBS. Consecutive sections were used for Acid Fuchsin Orange G (AFOG), Hart's elastin, and Movat's pentachrome stain using standard staining protocols.

2.5 Cardiomyocyte Size Measurement

Transgenic fish *Tg(myl7:actn3b-EGFP)*^{sd10}; *Tg(myl7:MKATE-CAAX)*^{sd11} were used in this experiment to analyze sarcomere structure and cell size. CMs were isolated according to the previous study (Sander, Sune, Jopling, Morera, & Izpisua Belmonte, 2013). Briefly, for each sample, the explanted ventricle was washed in heparin buffer (1× PBS plus 10 U/ml heparin and 100 U/ml penicillin-streptomycin), and then incubated in 250 μl digestion buffer (1× PBS plus 10 mM HEPES, 30 mM taurine, 5.5 mM glucose, 10 mM BDM, 12.5 μM $CaCl_2$, and collagenases II and IV (5 mg/ml each)) for 2 hours at 32°C in a 2 ml screw-cap tube. During incubation, the tubes were gently flipped every 10 minutes, and after incubation the mixture was gently pipetted up and down to completely dissociate the tissue. Then the homogeneous cell suspension was mixed with an equivalent volume of 4% paraformaldehyde (PFA), placed at room temperature for 10 minutes, and centrifuged at 250 × g for 5 minutes at room temperature. The supernatant was carefully removed and 250 μl DAPI (0.1 μg/ml) in Stop Buffer (1× PBS plus 10 mM HEPES, 30 mM taurine, 5.5 mM glucose, 10 mM BDM, and 12.5 μM $CaCl_2$) was added to the pellet and incubated for 10 minutes at room temperature. The samples were centrifuged again at 250 × g for 5 minutes at room temperature. The supernatant was carefully taken off and the pellet was resuspended in 30 μl of VECTASHIELD® Antifade Mounting Media (H-1000, Vector Laboratories) by gentle pipetting. The entire CM suspension was pipetted onto the slide and covered with cover glass. Slides were imaged using Nikon A1 outfitted with CFI Apochromat LWD 20× water immersion objective. CM areas were measured by ImageJ.

2.6 Immunofluorescence Staining

For localizing the PCNA signal, we used transgenic fish *Tg(fli1:nEGFP)*^{y7}*;Tg(-5.1myl7:nDsRed2)*^{f2}, which have endocardial/endothelial and myocardial nuclei highlighted with green and red fluorescence, respectively. Zebrafish heart explants were fixed in freshly-made 4% PFA at room temperature for 2 hours, then washed in PBS and immersed in 30% sucrose at 4°C for cryoprotection. Hearts were then embedded in cryomedium (Tissue-Tek® O.C.T. Compound, Sakura® Finetek, SAKURA FINETEK USA INC) and stored at -80°C. 14 μm frozen sections were cut on a cryotostat (Thermo Scientific FSE) and stored at -80°C for up to several months. For immunofluorescence staining, slides were retrieved and placed at room temperature for 30 minutes. Slides were then washed in PBS and incubated in mixture of 30% H_2O_2 :100% Methanol (1:9) for 45 minutes, washed in PBST (1×PBS plus 0.1% Tween-20) and incubated in blocking solution (5% goat serum in PBDT (PBS/ 0.1% tritonX-100/ 0.1% DMSO) for 1 hour at room temperature in a humidified box. PCNA antibody (P8825; Sigma, St. Louis, MO, USA) was diluted to 1:1500 with blocking solution and applied to the slides. Slides were incubated at 4°C in humidified box overnight. Slides were washed in PBST at 4°C on rocking platform in the dark, and then incubated in DAPI (0.1 μg/ml) plus goat anti-mouse Alexa Fluor 647 (1:200; A21235; Invitrogen) in blocking solution and at 4°C overnight. Slides were washed in PBST and mounted with VECTASHIELD® Antifade Mounting Media (H-1000, Vector Laboratories). Confocal images were acquired with a Nikon A1 outfitted with CFI Apochromat LWD 20x water immersion objective. Z series were obtained in 2 μm steps and spectral imaging with linear unmixing technique was used to eliminate autofluorescence according to manufacturer's instructions.

2.7 Statistics

Cardiac function and CM size data were statistically analyzed by two-tailed unpaired student t-test with significance set at $p < 0.05$. Graphs of data were generated by Prism7 (GraphPad, San Diego, CA, USA).

3.0 Results

3.1 Cardiac Functional Changes in *bmp10* mutants

bmp10 mutants have supra-normal cardiac outputs, which exceed the pumping capacity of the heart.

We hypothesized that due to the dilated hemorrhagic vessels and the resultant anemia, the *bmp10* mutant may have a high cardiac output state. To test this hypothesis, we performed echocardiographic studies in phenotypic *bmp10* mutants and WT siblings at 3, 5, and 12 months (mixture of males and females). As the zebrafish heart is highly trabeculated, instead of using a method developed for compacted mammalian heart, we calculated stroke volume by multiplying the ventricular outflow tract (VOT) area and the velocity time integral of blood flow across the VOT. Also, considering the fish body size may be a confounding factor, we normalized the volume data to the total body weight. At all timepoints, *bmp10* mutants exhibited a trend toward elevated stroke volume compared to WT sib, with significant increases at 3 and 12 months but not at 5 months (Fig. 2A). However, when normalized to body weight, stroke volume was significantly increased in *bmp10* mutants at all time points (Fig. 2B). The effect on stroke volume was particularly striking at 3 months, suggesting that earlier onset phenotype is associated with increased severity of heart dysfunction. Cardiac output in *bmp10* mutants is significantly higher at 3 and 5 months but not at 12 months, if total body weight is taken into account (Fig. 2C, D). Slow heart rates were also detected in *bmp10* mutants at 3 and 5 months. All data regarding cardiac output are summarized in Tables 1-3. Fractional shortening remains unchanged at all the time points (see Supplemental Tables 1-3). Taken together, the results suggest that volume overload due to decreased

vascular resistance leads to cardiac enlargement and a high output state. As such, these data suggest that this *bmp10* mutant is a good model for HOHF associated with HHT.

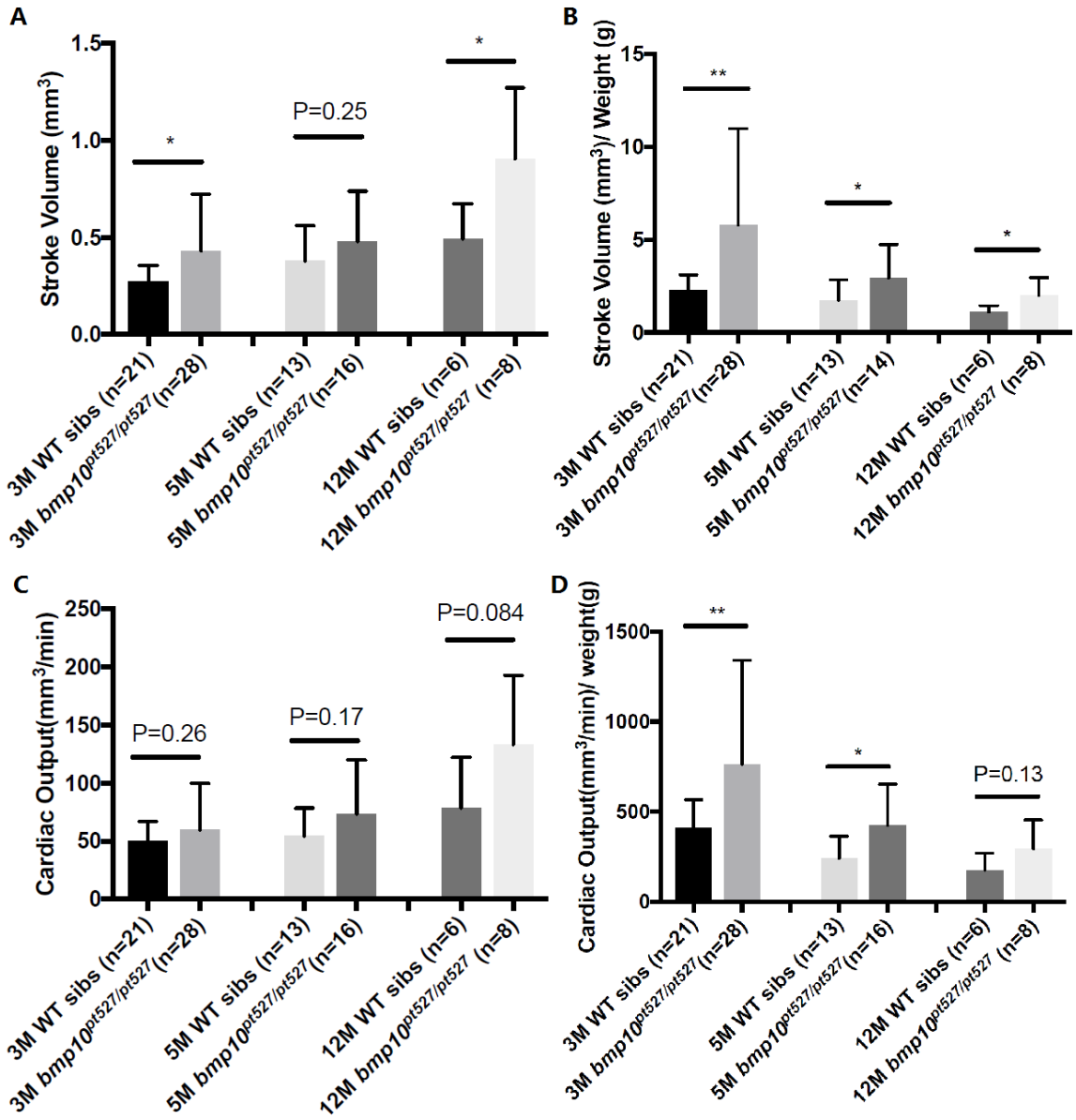

Figure 2. Stroke volume and cardiac output of *bmp10* mutants.

Echocardiography was performed in *bmp10* mutants with phenotype and the WT siblings at 3, 5 and 12 months. (A) Stroke volume in *bmp10* mutants was elevated at 3 and 12 months, but not at 5 months.
(B) Higher stroke volume in *bmp10* mutants at all time points, when data were indexed to total body weight.
(C) Cardiac output (stroke volume × heart rate) is not significantly different between groups.
(D) A high cardiac output state was observed in *bmp10* mutant at 3 and 5 months in indexed data. Data are mean ± s.d.; two tailed unpaired t-test, *$p < 0.05$, **$p < 0.01$. 3 months: N = 21 (WT, 16 males, 5 females) & 28 (*bmp10* mutant, 25 males, 3 females). 5 months: N = 13 (WT, 11 males, 2 females) and 16 (*bmp10* mutant, 13 males, 3 females). 12 months: N = 6 (WT, all males) and 8 (*bmp10* mutant, all males). Experimental repeats: 3 (3 months); 2 (5 months); 1 (12 months).

Table 1. 3 months *bmp10* mutants' body weight and cardiac parameters

Parameter	WT (n=21)	*bmp10*$^{pt527/pt527}$ (n=28)	p value*
Total body weight (g)	0.13±0.05	0.09±0.07	0.04
Heart rate (bpm)	180.89±25.54	140.93± 38.34	<0.001[b]
Ventricular Outflow tract diameter (mm)	0.24±0.03	0.24±0.04	0.99
Velocity time integral (mm)	6.21±2.13	9.28±5.72	0.013
Stroke volume (mm^3)	0.27±0.08	0.43±0.29	0.011
SV / weight ($mm^3\ g^{-1}$)	2.28±0.83	5.40±3.08	0.001[a]
Cardiac output ($mm^3\ min^{-1}$)	49.95±16.86	59.58±40.06	0.25
Cardiac output / weight ($mm^3 min^{-1}\ g^{-1}$)	410.98±155.13	764.85±576.65	0.004[a]

Table 2. 5 months *bmp10* mutants' body weight and cardiac parameters

Parameter	WT (n=17)	*bmp10*$^{pt527/pt527}$ (n=20)	p value*
Total body weight (g)	0.12±0.04	0.08±0.06	0.03
Heart rate (bpm)	180.10±25.35	132.95±31.68	<0.001[b]
Ventricular Outflow tract diameter (mm)	0.25±0.03	0.25±0.04	0.61
Velocity time integral (mm)	5.60±1.72	7.14±3.92	0.14
Stroke volume (mm^3)	0.27±0.09	0.40±0.29	0.088
SV / weight ($mm^3\ g^{-1}$)	2.28±0.83	5.23±3.50	0.0025[a]
Cardiac output ($mm^3\ min^{-1}$)	48.19±18.18	51.11±36.98	0.76
Cardiac output / weight ($mm^3\ min^{-1}\ g^{-1}$)	412.54±163.27	698.07±515.41	0.037[a]

Table 3. 12 months *bmp10* mutants' body weight and cardiac parameters

Parameter	WT (n=6)	*bmp10*$^{pt527/pt527}$ (n=8)	p value*
Total body weight (g)	0.45±0.07	0.48±0.16	0.67
Heart rate (bpm)	152.61±27.58	144.96±25.42	0.60[a]
Ventricular Outflow tract diameter (mm)	0.28±0.03	0.29±0.02	0.51
Velocity time integral (mm)	7.77±2.14	13.66±5.62	0.02
Stroke volume (mm^3)	0.49±0.18	0.91±0.36	0.03
SV / weight ($mm^3\ g^{-1}$)	1.10±0.35	2.00±0.95	0.04[a]
Cardiac output ($mm^3\ min^{-1}$)	78.70±43.54	133.18±59.55	0.08
Cardiac output / weight ($mm^3\ min^{-1}\ g^{-1}$)	175.35±93.90	295.16±157.45	0.13

* Unpaired t-test used to compare means between groups

Parameter values given as mean ± s.d.

a. agree with the HOHF clinical findings

b. do not agree with the HOHF clinical findings

3.2 Morphological Changes in *bmp10* mutants

bmp10 mutant early-onset vascular phenotype is associated with CM disorganization.

In our ultrasound study, hyperdynamic circulation and an enlarged, rounded ventricle are observed in *bmp10* mutants, with earlier onset phenotype being more severe than later onset phenotype. I hypothesized that the shape change in the *bmp10* mutant heart represents a structural adaptation that allows for a higher cardiac stroke volume. Therefore, I analyzed the ultrastructure of the ventricle in phenotypic *bmp10* mutant hearts compared to their WT siblings. I found that the structural changes in *bmp10* mutant hearts do not represent a progressive phenotype, and that earlier age of onset correlates with worse outcome.

Before 6 weeks, the zebrafish ventricle is comprised of a single-cell thick primordial layer and trabeculated myocardium, while after 6 weeks, an additional layer called the cortical layer covers the ventricle wall (Gupta & Poss, 2012) (Fig. 3). At 3 months, the outermost muscle layer of the ventricle wall of the phenotypic *bmp10* mutant was the primordial layer (11/11), whereas a minority of the wild-type siblings presented with a newly-developed cortical layer enveloping the heart (2/8) (Fig. 4A). In the trabeculated layer, the *bmp10* mutant hearts showed loosely compacted muscle, with larger spaces between the CMs (10/11) (Fig. 4A).

At 5 months, *bmp10* mutants' cortical layer was formed (3/3) (Fig. 4B), showing that loss of *bmp10* does not impair the ventricle's ability to develop a cortical layer. The role of the cortical layer is to strengthen the ventricle wall in response to the increased circulation demand as the fish grows (Gupta & Poss, 2012). With the cortical layer present, *bmp10* mutants' trabeculated layer is mildly affected, showing only small gaps between CMs (3/3) (Fig. 4B).

At 12 months, *bmp10* mutants have a relatively thick cortical layer (Fig. 4C) in 4/11 (36.4%), while WT siblings had a similar phenotype in 2/9 (22%). Only a mild change occurs in

the trabeculated layers of the *bmp10* mutant heart, with enlarged space between CMs (9/11) (Fig. 4C). Overall, my data suggest that the *bmp10* mutant heart has loosely organized CMs.

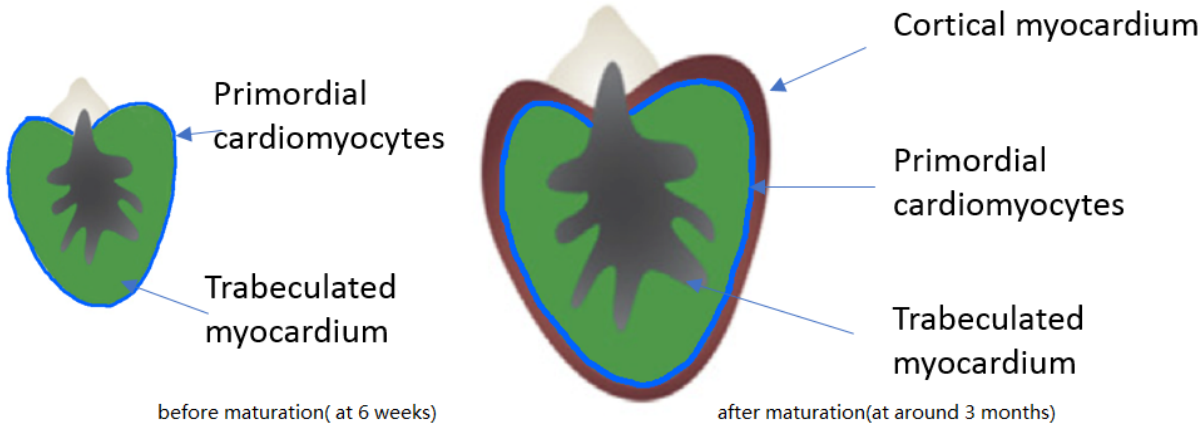

Figure 3. Juvenile zebrafish heart development.

(A) The 30 days ventricle has two muscle layers, trabeculated myocardium and primordial layer of single CM thickness.
(B) After juvenile organ maturation, ventricle is enveloped by an additional layer called cortical layer.

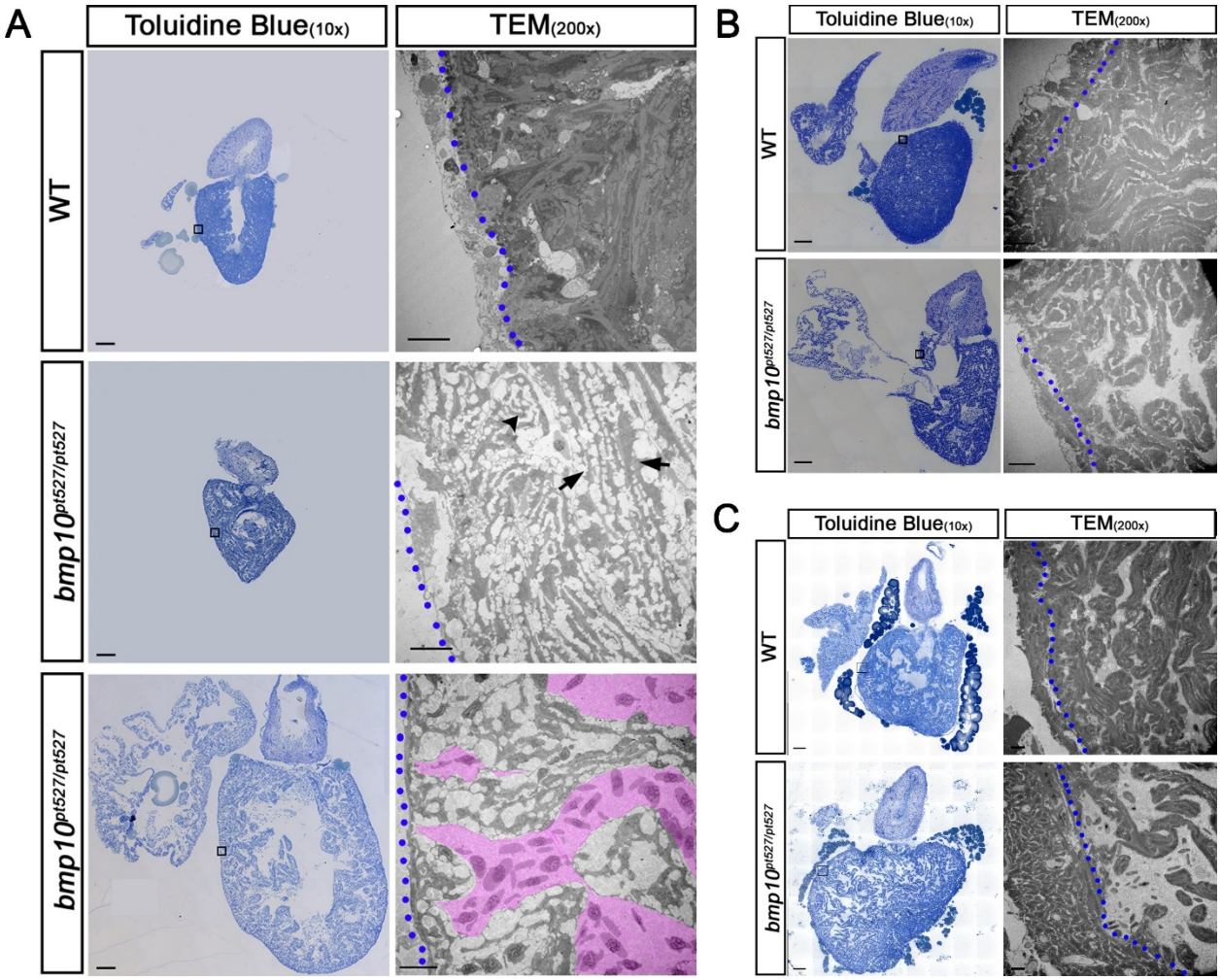

Figure 4. Structural changes in *bmp10* mutant heart.

Toluidine blue stained semi-thin epon sections and ultrathin TEM sections at 3 months (A), 5 months (B), and 12 months (C). Scale bars: 100 µm (toluidine blue); 10 µm (TEM).
(A) At 3 months, *bmp10* mutant has loosely arranged CMs in trabeculae. Arrows show laterally separated CMs; arrowhead indicates loosely connected CMs. In *bmp10* mutants, the ventricle wall is comprised of primordial layer of single CM thickness; while in the WT sibling, the ventricle is enveloped by cortical layer. Blue dotted lines, boundary of trabeculated layer; pink area, ventricle cavity. Tolidine blue: N = 8 (WT) and 11 (*bmp10* mutant); 2 experiments. TEM, N = 3 (WT) and 3 (*bmp10* mutant); 1 experiment.
(B) At 5 months, wider space is seen between trabeculae and CMs in *bmp10* mutant. Cortical layer is developed in both groups. Toluidine blue & TEM: N = 3 (WT) and 3 (*bmp10* mutant); 1 experiment for each.
(C) At 12 months, cortical layer muscle is mildly affected in *bmp10* mutant, with gaps between CMs. Toluidine blue: N = 9 (WT) and 11 (*bmp10* mutant); 2 experiments. TEM: N = 3 (WT) and 3 (*bmp10* mutant), 1 experiment.

3.3 Extracellular Matrix Deposition in *bmp10* mutant

Extracellular matrix changes are not apparent in *bmp10* mutant hearts.

Because I detected large gaps between CMs in *bmp10* mutants, I hypothesized that the gaps were filled with extracellular matrix. However, histological staining revealed no changes in collagen, elastin or proteoglycan deposition in *bmp10* mutant hearts at 3 or 5 months. (Supp. Fig. 1 and Fig. 5)

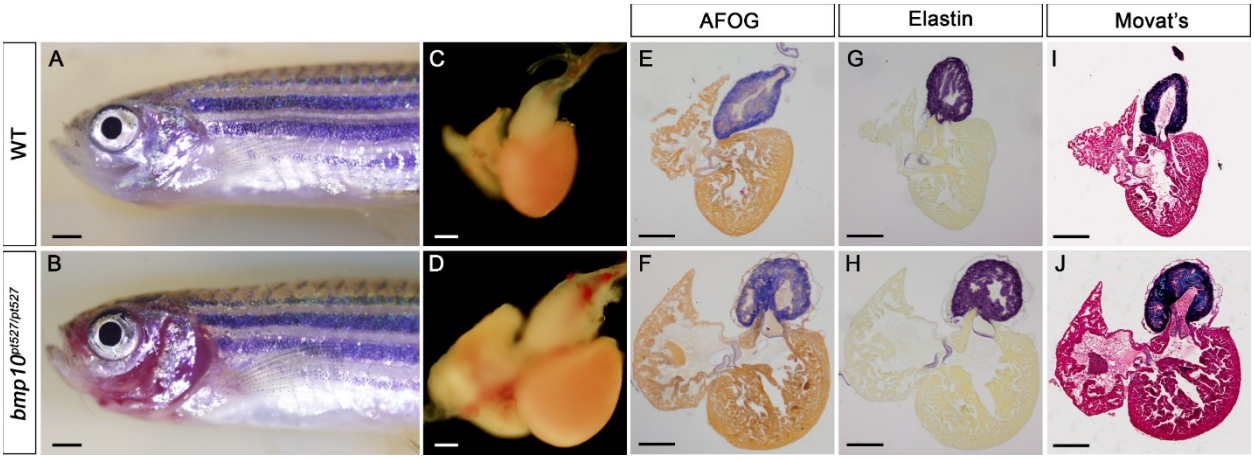

Figure 5. Extracellular matrix component deposition in the WT sibling and *bmp10* mutant heart at 5 months.

No abnormal deposition of collagen, elastin or proteoglycan in the ventricle remodeling of *bmp10* mutant at 5 months.
(A, B) Appearance of the WT sib and *bmp10* mutant. Scale bars: 1 mm
(C, D) Heart explants from fish in A and B. Scale bars: 200 µm
(E, F) AFOG stained sections. Blue: collagen; red: fibrin; orange: muscle. Scale bars: 200 µm.
(G, H) Hart's Elastin stained sections. Purple: elastin; yellow: counterstain. Scale bars: 200 µm.
(I, J) Movat's stained sections. Black: nuclei, elastic fiber; yellow: collagen fiber, reticular fiber; blue: ground substance, mucin; bright red: fibrin; red: muscle. Scale bars: 200 µm.
N = 3 (WT) and 3 (*bmp10* mutant). 3 sections per heart. 1 experiment for each staining.

3.4 Cardiomyocyte Hypertrophy in *bmp10* mutant

In *bmp10* mutants, CM size is increased while CMs remain mononucleated and sarcomere structure is normal.

An abnormally shaped heart with or without enlargement is seen in *bmp10* mutants, as well as altered cardiac function. I hypothesized that CM size is increased, and this

contributes to the functional and structural changes in *bmp10* mutant heart. To analyze CM size and their sarcomere organization, I isolated CMs from adult zebrafish ventricle and analyzed the size with the aid of transgenes highlighting alpha-actinin (EGFP) and cell membrane (mKATE) in green and red, respectively. At 5 months, CMs of the *bmp10* mutant heart tended to be larger than those of WT sibs, but this difference did not reach statistical significance. All of the CMs had a single nucleus, suggesting no endoreplication or dysregulation of cell cycle. Moreover, I detected no qualitative change in alpha-actinin organization in the sampled *bmp10* mutant CMs (Fig. 6A). However, due to the experiment procedure, I suspect that impaired/dead CMs might have been removed with supernatant, and thus those with myofilament disorganization are not detected in the samples. Together, my data suggest *bmp10* mutant may have CM hypertrophy to achieve increases in organ mass.

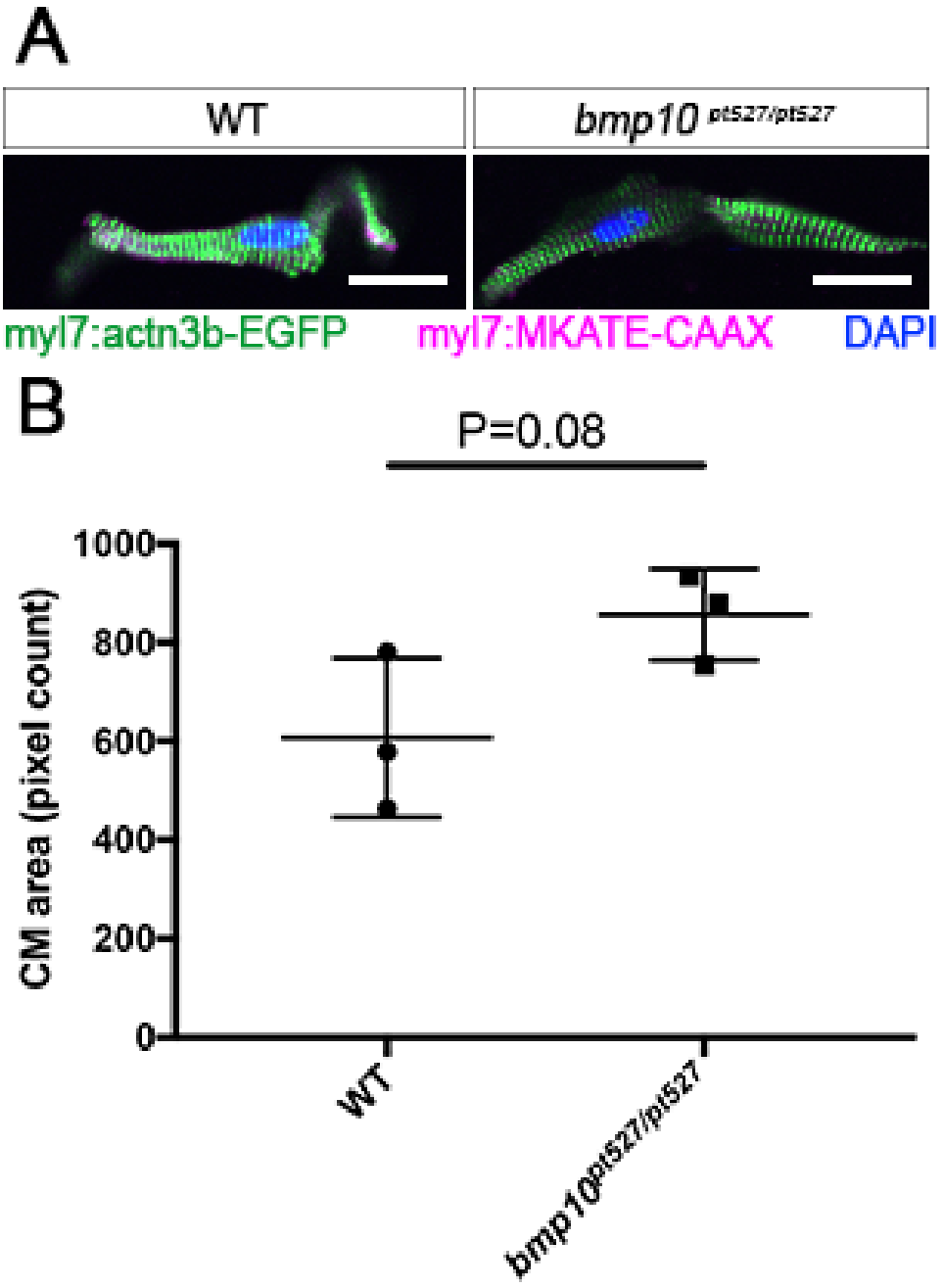

Figure 6. CM hypertrophy in *bmp10* mutant at 5 months.

(A) Representative images of CMs from WT and *bmp10* mutant ventricles, 5 months. Green: *Tg(myl7:actn3b-EGFP)*^{sd10} (Z-disc); magenta: *Tg(myl7: mKATE-CAAX)*^{sd11} (CM membrane); blue: DAPI (nucleus). Scale bar: 20 μm.
(B) CM area. WT: n = 3 hearts, 8-30 CMs/heart. *bmp10* mutant: n = 3 hearts, 90-155 CMs/heart. 1 experiment.

3.5 Proliferation or DNA Damage in *bmp10* mutant Heart

bmp10 mutant hearts have elevated staining of PCNA in endocardial and myocardial cells.

To dissect cellular changes in *bmp10* mutant heart, I stained hearts for PNCA. At 3 months, PCNA signals were associated with edema in the mutants (6/6) (Fig. 7A, B, K, & L). Qualitative analysis of colocalization revealed enhanced proliferation in endocardial *[Tg(fli1a: nEFGP)^{y7}*; 5/6] and myocardial [*Tg (cmlc2:nDsRed2)^{f2}*; 3/6] cells (Fig. 7C-H); the remaining mutant showed increased PCNA signal that failed to colocalize with either cell type. All analyzed fish showed edema, indicative of poor heart function (Fig. 7K, &L).

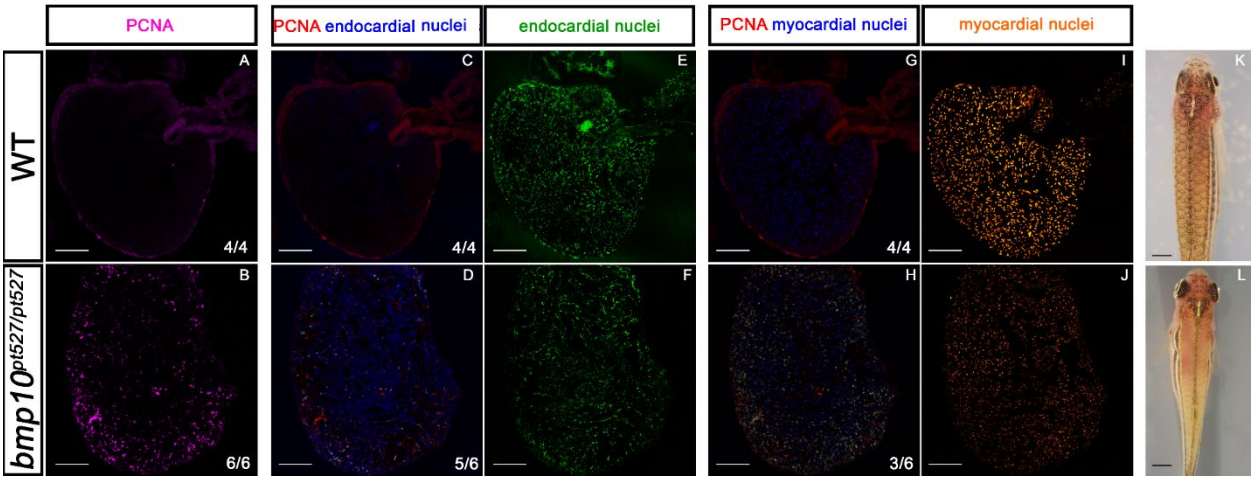

Figure 7. Increased PCNA in *bmp10* mutant heart at 3 months.

(A, B) PNCA signal is largely increased in *bmp10* mutant heart. Magenta: overall PCNA signal in heart. Scale bars: 100 μm.
(C, D) Sparse PCNA signals overlap with endocardial nuclei. Red: PCNA; blue: endocardial nuclei; white: overlapping signal; pseudocolored by colocalization analysis in ImageJ.
(E, F) green: endocardial nuclei
(G, H) PCNA signals overlap with myocardial nuclei. Red: PCNA; blue: myocardial nuclei; white: overlapping signal; pseudocolored by colocalization analysis in ImageJ.
(I, J) orange: myocardial nuclei
(K, L) *bmp10* mutant with increased PCNA showed edema. Scale bars: 1 mm. N = 4 (WT) and 6 (*bmp10* mutant) hearts, 3 sections per heart. 1 experiment.

4.0 Discussion

The central finding of this study is that depletion of *bmp10* leads to dilated and hemorrhagic vasculature and induces HOHF. We think the zebrafish *bmp10* mutant may serve as a valuable model for HOHF.

In this study, we detected increased stroke volume index and preserved fractional shortening at all the time points in *bmp10* mutants. These results are consistent with the clinical findings in HOHF. In *bmp10* mutants, the early onset of the vascular abnormality is correlated with a more severe outcome in terms of changes in stroke volume and the overall well-being of the fish, such as showing raised scales. This could be explained by the timing of cortical layer development, a maturation process of the ventricle in juvenile zebrafish that serves to strengthen the ventricle wall and to meet the increased hemodynamic need (Gupta & Poss, 2012). If *bmp10* mutants develop AVMs before the formation of the cortical layer, the ventricle wall of single CM thickness may not be able to compensate for the volume overload. Surprisingly, the vascular phenotype is also correlated with lower heart rate in *bmp10* mutants. However, I suspect that the slow heart beat in *bmp10* mutants may be due to the increased susceptibility of *bmp10* mutants to anesthesia.

High cardiac output is generated by the heart with increased organ size and preserved systolic function in *bmp10* mutants. The heart of phenotypic *bmp10* mutants is large compared to body size. At the cellular level, preliminary data suggest that CMs are hypertrophic and the space between CMs is enlarged. I suspect that increasing CM volume and extracellular space reflects ventricular remodeling to increase organ mass. However, collagen is not deposited in the ventricle tissue, indicating no fibrosis. This is consistent with the fractional shortening data showing that

the *bmp10* mutant heart has preserved contractility and systolic function. The echocardiography and collagen data in zebrafish *bmp10* mutants agree with the clinical findings in HOHF, suggesting that the *bmp10* mutant is a good model for HOHF.

PCNA is detected in the ventricle of *bmp10* mutants with edema. PNCA is a marker for proliferation while ubiquityl-PCNA is associated with DNA damage (Kanao et al., 2015). Our PCNA antibody detects both, so additional experiments will be necessary to differentiate these two possibilities. DNA damage may result from replication stress on DNA molecules or from mitochondrial dysfunction, as the *bmp10* mutant heart is working harder, and mitochondria may not be able to make enough ATP, leading to reactive oxygen species (ROS) production and DNA damage. The PCNA signal is found in the at least two cell types, marked by a *fli1a*-driven transgene (endocardial or endothelial cells) or a *myl7*-driven transgene (CMs). Anti-PCNA signal in endocardial nuclei is sparse but detected in most samples. PCNA signal colocalizing with myocardial nuclei is present in half of the samples. Future work will be needed to determine whether enhanced PCNA expression is a protective or pathological response in the heart, and whether other gene expression changes are detectable in the *bmp10* mutant heart, such as changes in CM contractility markers or sodium channels.

Overall, these data show that the zebrafish *bmp10* mutant is a useful HOHF model, and with this model we gain insights into the cardiac remodeling in HOHF. In our zebrafish model, HOHF is associated with increased heart size (Fig. 8A). At the tissue level, muscle fibers are separated, the extracellular space is increased, and multiple cells types are PCNA-positive, suggesting either proliferation or DNA damage (Fig. 8B). Further work is required to understand how these morphological changes lead to increased cardiac output in response to low systemic vascular resistance.

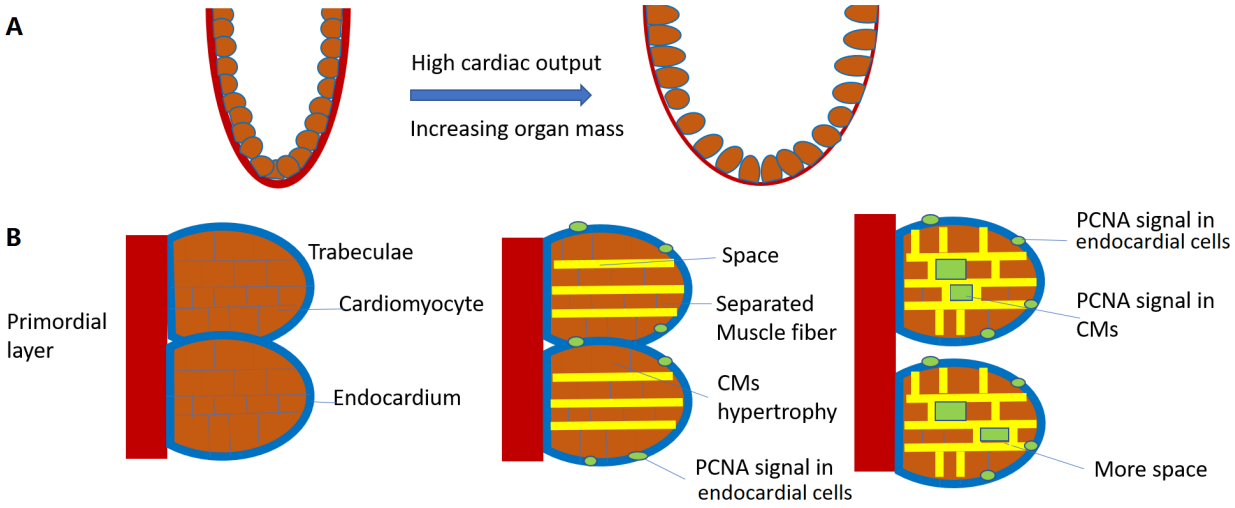

Figure 8. Model of cardiac remodeling in HOHF

(A) Association of HOHF and increased heart size.
(B) Morphological elements and molecular change in HOHF

Appendix A Supplemental Figure

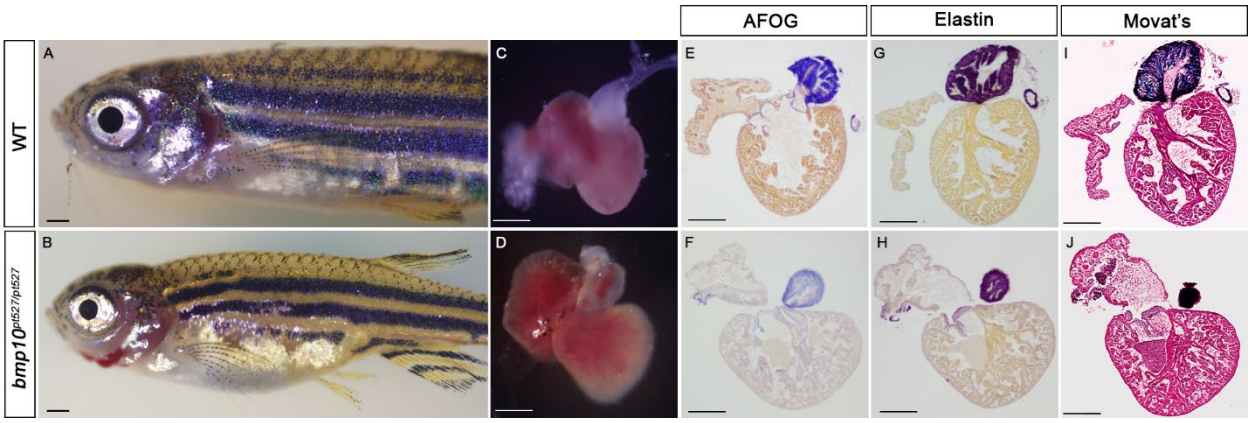

Supplemental Figure 1. Extracellular matrix component deposition in the WT sibling and *bmp10* mutant heart at 3 months.

No abnormal deposition of collagen, elastin or proteoglycan in the ventricle remodeling of *bmp10* mutant at 3 months.
(A, B) Appearance of the WT sib and *bmp10* mutant. Scale bars: 1 mm.
(C, D) Heart explants from fish in A and B. Scale bars: 200 μm.
(E, F) AFOG stained sections. Blue: collagen; red: fibrin; orange: muscle. Scale bars: 200 μm.
(G, H) Hart's Elastin stained sections. Purple: elastin; yellow: counterstain. Scale bars: 200 μm.
(I, J) Movat's stained sections. Black: nuclei, elastic fiber; yellow: collagen fiber, reticular fiber; blue: ground substance, mucin; bright red: fibrin; red: muscle. Scale bars: 200 μm.
N=3 (WT) and 3(*bmp10* mutant). 3 sections per heart. 1 experiment for each staining.

Appendix B Supplemental Tables

Supplemental Table 1. 3 months *bmp10* mutants cardiac diameters and fractional shortening

Parameter	WT (n=17)	*bmp10*$^{pt527/pt527}$ (n=20)	p value*
End-systolic diameter (mm)	0.66±0.14	0.74±0.19	0.16
End-diastolic diameter (mm)	0.84± 0.16	0.97±0.22	0.05
Fractional shortening (%)	21.10±3.77	23.37±7.63	0.27[a]

Supplemental Table 2. 5 months *bmp10* mutants cardiac diameters and fractional shortening

Parameter	WT (n=10)	*bmp10*$^{pt527/pt527}$ (n=10)	p value*
End-systolic diameter (mm)	0.85±0.09	0.86±0.14	0.84
End-diastolic diameter (mm)	1.06±0.10	1.09± 0.12	0.58
Fractional shortening (%)	19.40±5.58	20.83±7.99	0.65[a]

Supplemental Table 3. 12 months *bmp10* mutants cardiac diameters and fractional shortening

Parameter	WT (n=6)	*bmp10*$^{pt527/pt527}$ (n=8)	p value*
End-systolic diameter (mm)	1.14±0.19	1.09±0.16	0.64
End-diastolic diameter (mm)	1.44±0.16	1.35± 0.17	0.33
Fractional shortening (%)	21.11±6.06	19.07±4.36	0.47[a]

* Unpaired t-test used to compare means between groups
Parameter values given as mean ± s.d.
a. agree with the HOHF clinical findings

Bibliography

Anand, I. S., & Florea, V. G. (2001). High Output Cardiac Failure. *Curr Treat Options Cardiovasc Med, 3*(2), 151-159.

Aurigemma, G. P., Zile, M. R., & Gaasch, W. H. (2006). Contractile behavior of the left ventricle in diastolic heart failure: with emphasis on regional systolic function. *Circulation, 113*(2), 296-304. doi:10.1161/circulationaha.104.481465

Brown MA, Zhao Q, Baker KA, Naik C, Chen C, Pukac L, Singh M, Tsareva T, Parice Y, Mahoney A, et al. (2005) Crystal structure of BMP-9 and functional interactions with pro-region and receptors. J Biol Chem. 280(26):25111–25118. doi: 10.1074/jbc.M503328200.

Burggren WW, Pinder AW. (1991). Ontogeny of cardiovascular and respiratory physiology in lower vertebrates. Annu Rev Physiol 53: 107–153

Castonguay, R., Werner, E. D., Matthews, R. G., Presman, E., Mulivor, A. W., Solban, N., . . . Grinberg, A. V. (2011). Soluble endoglin specifically binds bone morphogenetic proteins 9 and 10 via its orphan domain, inhibits blood vessel formation, and suppresses tumor growth. *J Biol Chem, 286*(34), 30034-30046. doi:10.1074/jbc.M111.260133

Chatterjee, K. (2012). Pathophysiology of systolic and diastolic heart failure. *Med Clin North Am, 96*(5), 891-899. doi:10.1016/j.mcna.2012.07.001

Chen, H., Brady Ridgway, J., Sai, T., Lai, J., Warming, S., Chen, H., . . . Yan, M. (2013). Context-dependent signaling defines roles of BMP9 and BMP10 in embryonic and postnatal development. *Proc Natl Acad Sci U S A, 110*(29), 11887-11892. doi:10.1073/pnas.1306074110

Chen, H., Shi, S., Acosta, L., Li, W., Lu, J., Bao, S., . . . Shou, W. (2004). BMP10 is essential for maintaining cardiac growth during murine cardiogenesis. *Development, 131*(9), 2219-2231. doi:10.1242/dev.01094

Corti, P., Young, S., Chen, C. Y., Patrick, M. J., Rochon, E. R., Pekkan, K., & Roman, B. L. (2011). Interaction between alk1 and blood flow in the development of arteriovenous malformations. Development (Cambridge, England), 138(8), 1573–1582. doi:10.1242/dev.060467

David L, Mallet C, Mazerbourg S, Feige JJ, Bailly S. (2007). Identification of BMP9 and BMP10 as functional activators of the orphan activin receptor-like kinase 1 (ALK1) in endothelial cells. Blood. 109(5):1953–1961. doi: 10.1182/blood-2006-07-034124.

Gallione CJ, Repetto GM, Legius E, et al. (2004). A combined syndrome of juvenile polyposis and hereditary haemorrhagic telangiectasia associated with mutations in MADH4 (SMAD4). Lancet. 363 (9412): 852–9.

Garcia-Tsao, G. (2007). Liver involvement in hereditary hemorrhagic telangiectasia (HHT). *J Hepatol, 46*(3), 499-507. doi:10.1016/j.jhep.2006.12.008

Gaussin, V., Van de Putte, T., Mishina, Y., Hanks, M. C., Zwijsen, A., Huylebroeck, D., . . . Schneider, M. D. (2002). Endocardial cushion and myocardial defects after cardiac myocyte-specific conditional deletion of the bone morphogenetic protein receptor ALK3. *Proc Natl Acad Sci U S A, 99*(5), 2878-2883. doi:10.1073/pnas.042390499

González-Rosa, J. M., Burns, C. E., & Burns, C. G. (2017). Zebrafish heart regeneration: 15 years of discoveries. Regeneration (Oxford, England), 4(3), 105–123. doi:10.1002/reg2.83

Gupta, V., & Poss, K. D. (2012). Clonally dominant cardiomyocytes direct heart morphogenesis.

Nature, 484(7395), 479-484. doi:10.1038/nature11045
Johnson DW, Berg JN, Baldwin MA, et al. (1996). Mutations in the activin receptor-like kinase 1 gene in hereditary haemorrhagic telangiectasia type 2. Nat. Genet. 13 (2): 189–95.
Kanao R., Masutani C. (2017). Regulation of DNA damage tolerance in mammalian cells by post-translational modifications of PCNA. Mutat. Res. 803–805:82–88
Kossack, M., Hein, S., Juergensen, L., Siragusa, M., Benz, A., Katus, H. A., . . . Hassel, D. (2017). Induction of cardiac dysfunction in developing and adult zebrafish by chronic isoproterenol stimulation. *J Mol Cell Cardiol, 108*, 95-105. doi:10.1016/j.yjmcc.2017.05.011
Laux, D. W., Young, S., Donovan, J. P., Mansfield, C. J., Upton, P. D., & Roman, B. L. (2013). Circulating Bmp10 acts through endothelial Alk1 to mediate flow-dependent arterial quiescence. *Development, 140*(16), 3403-3412. doi:10.1242/dev.095307
Massague, J. (2012). TGFbeta signalling in context. *Nat Rev Mol Cell Biol, 13*(10), 616-630. doi:10.1038/nrm3434
Mazerbourg, S., Sangkuhl, K., Luo, C. W., Sudo, S., Klein, C., & Hsueh, A. J. (2005). Identification of receptors and signaling pathways for orphan bone morphogenetic protein/growth differentiation factor ligands based on genomic analyses. *J Biol Chem, 280*(37), 32122-32132. doi:10.1074/jbc.M504629200
McAllister KA, Grogg KM, Johnson DW, et al. (1994). Endoglin, a TGF-beta binding protein of endothelial cells, is the gene for hereditary haemorrhagic telangiectasia type 1. Nat. Genet. 8 (4): 345–51.
Mehta, P. A., & Dubrey, S. W. (2009). High output heart failure. *Qjm, 102*(4), 235-241. doi:10.1093/qjmed/hcn147
Neuhaus, H., Rosen, V., & Thies, R. S. (1999). Heart specific expression of mouse BMP-10 a novel member of the TGF-beta superfamily. *Mech Dev, 80*(2), 181-184.
Nguyen, C. T., Lu, Q., Wang, Y., & Chen, J. N. (2008). Zebrafish as a model for cardiovascular development and disease. *Drug Discov Today Dis Models, 5*(3), 135-140. doi:10.1016/j.ddmod.2009.02.003
Okagawa, H., Markwald, R. R., & Sugi, Y. (2007). Functional BMP receptor in endocardial cells is required in atrioventricular cushion mesenchymal cell formation in chick. *Dev Biol, 306*(1), 179-192. doi:10.1016/j.ydbio.2007.03.015
Reddy, Y. N. V., Melenovsky, V., Redfield, M. M., Nishimura, R. A., & Borlaug, B. A. (2016). High-Output Heart Failure: A 15-Year Experience. *J Am Coll Cardiol, 68*(5), 473-482. doi:10.1016/j.jacc.2016.05.043
Roman, B. L., & Hinck, A. P. (2017). ALK1 signaling in development and disease: new paradigms. Cellular and molecular life sciences : CMLS, 74(24), 4539–4560. doi:10.1007/s00018-017-2636-4
Rossi, A., Cicoira, M., Golia, G., Zanolla, L., Franceschini, L., Marino, P., . . . Zardini, P. (2004). Amino-terminal propeptide of type III procollagen is associated with restrictive mitral filling pattern in patients with dilated cardiomyopathy: a possible link between diastolic dysfunction and prognosis. *Heart, 90*(6), 650-654.
Sander, V., Sune, G., Jopling, C., Morera, C., & Izpisua Belmonte, J. C. (2013). Isolation and in vitro culture of primary cardiomyocytes from adult zebrafish hearts. *Nat Protoc, 8*(4), 800-809. doi:10.1038/nprot.2013.041
Savarese, G., & Lund, L. H. (2017). Global Public Health Burden of Heart Failure. *Card Fail Rev, 3*(1), 7-11.
Sedmera D, Thomas PS. (1996). Trabeculation in the embryonic heart. Bioessays. Epub, 18(7):607,

1996/07/01. eng.
Shovlin, C. L. (2015). Circulatory contributors to the phenotype in hereditary hemorrhagic telangiectasia. *Front Genet, 6*, 101. doi:10.3389/fgene.2015.00101
Sun, X., Hoage, T., Bai, P., Ding, Y., Chen, Z., Zhang, R., . . . Xu, X. (2009). Cardiac hypertrophy involves both myocyte hypertrophy and hyperplasia in anemic zebrafish. *PLoS One, 4*(8), e6596. doi:10.1371/journal.pone.0006596
Wang, L. W., Huttner, I. G., Santiago, C. F., Kesteven, S. H., Yu, Z. Y., Feneley, M. P., & Fatkin, D. (2017). Standardized echocardiographic assessment of cardiac function in normal adult zebrafish and heart disease models. *Dis Model Mech, 10*(1), 63-76. doi:10.1242/dmm.026989
Woods, I. G., Wilson, C., Friedlander, B., Chang, P., Reyes, D. K., Nix, R., Kelly, P. D., Chu, F., Postlethwait, J. H. and Talbot, W. S. (2005). The zebrafish gene map defines ancestral vertebrate chromosomes. Genome Res. 15, 1307-1314.